 CMES, vol.88, no.1, pp.29-47, 2012

The Jordan Structure of Residual Dynamics Used to Solve Linear Inverse Problems

Chein-Shan Liu[1], **Su-Ying Zhang**[2] **and Satya N. Atluri**[3]

Abstract: With a detailed investigation of n linear algebraic equations $\mathbf{Bx}=\mathbf{b}$, we find that the scaled residual dynamics for $\mathbf{y}\in\mathbb{S}^{n-1}$ is equipped with four structures: the Jordan dynamics, the rotation group $SO(n)$, a generalized Hamiltonian formulation, as well as a metric bracket system. Therefore, it is the first time that we can compute the steplength used in the iterative method by a novel algorithm based on the Jordan structure. The algorithms preserving the length of $\mathbf{y}$ are developed as the structure preserving algorithms (SPAs), which can significantly accelerate the convergence speed and are robust enough against the noise in the numerical solutions of ill-posed linear inverse problems.

Keywords: Ill-posed linear system, Future cone, Jordan dynamics, Generalized Hamiltonian formulation, Metric bracket system, Linear inverse problems, Structure preserving algorithms (SPAs)

1 Introduction

In this paper we investigate the residual dynamics of the residual vector:

$$\mathbf{r}=\mathbf{Bx}-\mathbf{b} \tag{1}$$

for a linear algebraic equations system:

$$\mathbf{Bx}=\mathbf{b}, \tag{2}$$

where $\mathbf{x}\in\mathbb{R}^n$ is an unknown vector, to be determined from a given coefficient matrix $\mathbf{B}\in\mathbb{R}^{n\times n}$ and the input $\mathbf{b}\in\mathbb{R}^n$. Eq. (2) might be an ill-posed system if it is used to solve the linear inverse problems of which the condition number Cond($\mathbf{B}$) is quite large.

[1] Department of Civil Engineering, National Taiwan University, Taipei, Taiwan. E-mail: liucs@ntu.edu.tw
[2] College of Physics and Electronic Engineering, Shanxi University, Taiyuan, China.
[3] Center for Aerospace Research & Education, University of California, Irvine

The relaxed steepest descent method (RSDM) to solve Eq. (2) is given by [Liu (2011a); Liu (2012a)]:
(i) Select a suitable value of $0 \leq \gamma < 1$ and give an initial $\mathbf{x}_0$, and then $\mathbf{R}_0 = \mathbf{C}\mathbf{x}_0 - \mathbf{b}_1$.
(ii) For $k = 0, 1, 2, \ldots$, we repeat the following computations:

$$\mathbf{x}_{k+1} = \mathbf{x}_k - (1-\gamma)\frac{\|\mathbf{R}_k\|^2}{\mathbf{R}_k^{\mathrm{T}}\mathbf{C}\mathbf{R}_k}\mathbf{R}_k, \tag{3}$$

$$\mathbf{R}_{k+1} = \mathbf{C}\mathbf{x}_{k+1} - \mathbf{b}_1. \tag{4}$$

If $\|\mathbf{R}_{k+1}\| < \varepsilon$ for a prescribed convergence criterion ε then stop; otherwise, go to step (ii). In the above, $\mathbf{C} = \mathbf{B}^{\mathrm{T}}\mathbf{B}$, $\mathbf{b}_1 = \mathbf{B}^{\mathrm{T}}\mathbf{b}$, $\mathbf{R}_k = \mathbf{B}^{\mathrm{T}}\mathbf{r}_k$, and $0 \leq \gamma < 1$ is a relaxation parameter.

To account of the sensitivity to noise it is often used a regularization method to solve the ill-posed problem [Kunisch and Zou (1998); Wang and Xiao (2001); Xie and Zou (2002); Resmerita (2005)], where a suitable regularization parameter is used to depress the bias in the computed solution by a better balance of approximation error and propagated data error. There are many methods developed after the pioneering work of Tikhonov and Arsenin (1977). Previously, the first author and his co-workers have developed several methods to solve the ill-posed linear problems, like that using the fictitious time integration method as a filter for ill-posed linear system [Liu and Atluri (2009a)], a modified polynomial expansion method [Liu and Atluri (2009b)], the non-standard group preserving scheme [Liu and Chang (2009)], a vector regularization method [Liu, Hong and Atluri (2010); Liu (2012b)], the relaxed steepest descent method [Liu (2011a, 2012a)], the optimal iterative algorithm [Liu and Atluri (2011)], the globally optimal iterative algorithm [Liu (2012c)], an adaptive Tikhonov regularization method [Liu (2012d)], an optimally generalized Tikhonov regularization method [Liu (2012e)], as well as an optimal tri-vector iterative algorithm [Liu (2012f)].

In this paper we will modify the steplength used in the iterative algorithm from a theoretical foundation of a future cone and the Jordan structure of a scaled residual vector $\mathbf{y} \in \mathbb{S}^{n-1}$. The remaining parts of this paper are arranged as follows. In Section 2 we start from a future cone in the Minkowski space to derive a system of nonlinear ODEs for the numerical solution of Eq. (2). Then, the scaled residual dynamics on the future cone is constructed in Section 3, resulting to a Jordan dynamics, a skew-symmetric dynamical system, a generalized Hamiltonian system and a metric bracket system. Accordingly, two structure preserving algorithms to solve Eq. (2) are developed in Section 4. The numerical examples of linear inverse problems are given in Section 5 to display some advantages of the newly developed structure preserving algorithms (SPAs). Finally, the conclusions are drawn in Sec-

tion 6.

2 A future cone in the Minkowski space

For Eq. (1) we can introduce a scalar function:

$$h(\mathbf{x},t) = \frac{1}{2}Q(t)\|\mathbf{r}(\mathbf{x})\|^2 - \frac{1}{2}\|\mathbf{r}_0\|^2 = 0, \tag{5}$$

where we let $\mathbf{x}$ be a function of a time-like variable t, with the initial values of $\mathbf{x}(0) = \mathbf{x}_0$ and $\mathbf{r}_0 = \mathbf{r}(\mathbf{x}_0)$, and $Q(t) > 0$ with $Q(0) = 1$ is a monotonically increasing function of t. In terms of

$$\mathbf{X} = \begin{bmatrix} \frac{\mathbf{r}}{\|\mathbf{r}_0\|} \\ \frac{1}{\sqrt{Q(t)}} \end{bmatrix}, \tag{6}$$

Eq. (5) represents a positive cone:

$$\mathbf{X}^{\mathrm{T}}\mathbf{g}\mathbf{X} = 0 \tag{7}$$

in the Minkowski space $\mathbb{M}^{n+1}$, which is endowed with an indefinite Minkowski metric tensor:

$$\mathbf{g} = \begin{bmatrix} \mathbf{I}_n & \mathbf{0}_{n\times 1} \\ \mathbf{0}_{1\times n} & -1 \end{bmatrix}, \tag{8}$$

where $\mathbf{I}_n$ is the $n \times n$ identity matrix. Because the last component $1/\sqrt{Q(t)}$ of $\mathbf{X}$ is positive, the cone in Eq. (7) is a future cone [Liu (2001)] as shown in Fig. 1.

When $Q > 0$, the manifold defined by Eq. (5) is continuous and differentiable, and as a consequence of the consistency condition, we have

$$\frac{1}{2}\dot{Q}(t)\|\mathbf{r}(\mathbf{x})\|^2 + Q(t)\mathbf{R}\cdot\dot{\mathbf{x}} = 0, \tag{9}$$

which is obtained by taking the differential of Eq. (5) with respect to t and considering $\mathbf{x} = \mathbf{x}(t)$ and $h(\mathbf{x},t) = 0$ for all t.

Corresponding to $\mathbf{r}$ in Eq. (1),

$$\mathbf{R} := \mathbf{B}^{\mathrm{T}}\mathbf{r} \tag{10}$$

is the steepest descent vector. We suppose that the evolution of $\mathbf{x}$ is driven by $\mathbf{R}$:

$$\dot{\mathbf{x}} = \lambda\mathbf{R}. \tag{11}$$

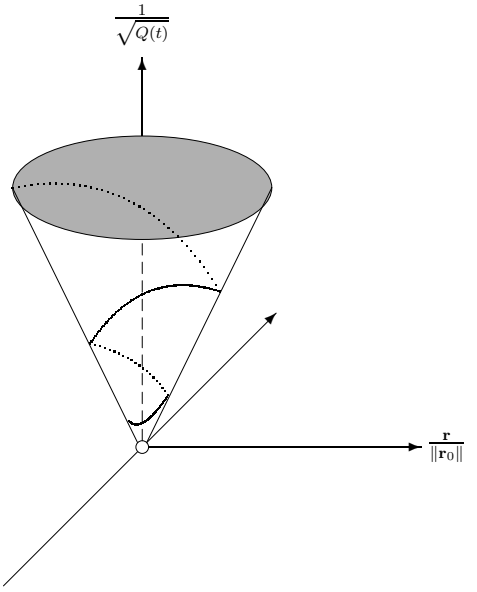

Figure 1: A cone structure in the Minkowski space for the evolution of residual dynamics of linear system.

Inserting Eq. (11) into Eq. (9) we can derive a nonlinear ODEs system:

$$\dot{\mathbf{x}} = -q(t)\frac{\|\mathbf{r}\|^2}{\mathbf{r}^{\mathrm{T}}\mathbf{A}\mathbf{r}}\mathbf{B}^{\mathrm{T}}\mathbf{r}, \tag{12}$$

where

$$\mathbf{A} := \mathbf{B}\mathbf{B}^{\mathrm{T}}, \tag{13}$$

$$q(t) := \frac{\dot{Q}(t)}{2Q(t)} > 0. \tag{14}$$

Hence, in our algorithm, if $Q(t)$ can be guaranteed to be a monotonically increasing function of t, we have an absolutely convergent property in solving the linear equations system (2):

$$\|\mathbf{r}(\mathbf{x})\|^2 = \frac{\|\mathbf{r}_0\|^2}{Q(t)}, \tag{15}$$

wherein we can observe that the path of $\mathbf{X}$ gradually tends down to the vertex point along the cone defined by Eq. (7) as schematically shown in Fig. 1. When the path of $\mathbf{r}$ reaches to the vertex point $\mathbf{r} = \mathbf{0}$, we can obtain the solution of $\mathbf{B}\mathbf{x} - \mathbf{b} = \mathbf{0}$.

3 Dynamics on the future cone

From Eq. (12) we can observe that it is utmost important to study the dynamics of $\mathbf{r}$ in order to have a better understanding of the solution behavior of $\mathbf{x}$. In order to keep $\mathbf{x}$ on the manifold (15) we can consider the evolution of $\mathbf{r}$ along the path $\mathbf{x}(t)$ of Eq. (12) by

$$\dot{\mathbf{r}} = \mathbf{B}\dot{\mathbf{x}} = -q(t)\frac{\|\mathbf{r}\|^2}{\mathbf{r}^{\mathrm{T}}\mathbf{A}\mathbf{r}}\mathbf{A}\mathbf{r}. \tag{16}$$

3.1 The Jordan dynamics

Let

$$\mathbf{y} = \mathbf{r}\sqrt{Q(t)} \tag{17}$$

be a scaled residual vector, and from Eq. (15) we know that $\mathbf{y} \in \mathbb{S}^{n-1}$ with a radius $\|\mathbf{r}_0\|$. At the same time, Eq. (12) can be written as

$$\dot{\mathbf{x}} = -q(t)\frac{\|\mathbf{y}\|^2}{\mathbf{y}^{\mathrm{T}}\mathbf{A}\mathbf{y}}\mathbf{B}^{\mathrm{T}}\mathbf{r}. \tag{18}$$

Below we will develop a new theory to compute the steplength:

$$q(t)\frac{\|\mathbf{y}\|^2}{\mathbf{y}^{\mathrm{T}}\mathbf{A}\mathbf{y}}.$$

Several modifications to the steepest descent method (SDM) have been recurred [Liu (2011a, 2012a)], which have stimulated a new interest in the SDM because it is recognized that the gradient vector itself is not a bad choice of the solution direction, but rather that the steplength:

$$\frac{\|\mathbf{R}\|^2}{\mathbf{R}^{\mathrm{T}}\mathbf{C}\mathbf{R}}$$

originally used in the SDM causes the slow convergence behavior. Barzilai and Borwein (1988) have presented a new choice of steplength through two-point step-size. But its performance and numerical stability are not good [Liu (2012d)].

Now we derive the governing equation for $\mathbf{y}$. From Eqs. (16), (17) and (14) we can derive

$$\dot{\mathbf{y}} = q(t)\left[\mathbf{I}_n - \frac{\|\mathbf{y}\|^2}{\mathbf{y}^{\mathrm{T}}\mathbf{A}\mathbf{y}}\mathbf{A}\right]\mathbf{y}. \tag{19}$$

If we define the following operator:

$$\mathbf{D} = \mathbf{I}_n - \frac{\|\mathbf{y}\|^2}{\mathbf{y}^{\mathrm{T}}\mathbf{A}\mathbf{y}}\mathbf{A}, \tag{20}$$

we have a new dynamical system for $\mathbf{y}$:

$$\dot{\mathbf{y}} = q(t)\mathbf{D}\mathbf{y}, \tag{21}$$

where $\mathbf{D}$ satisfies the following properties:

$$\mathbf{D}^{\mathrm{T}} = \mathbf{D}, \;\; \mathbf{y}^{\mathrm{T}}\mathbf{D}\mathbf{y} = 0, \tag{22}$$

due to $\mathbf{A}^{\mathrm{T}} = \mathbf{A}$.

Usually, if the length of $\mathbf{y}$ is preserved, the matrix $\mathbf{D}$ is skew-symmetric, but the present $\mathbf{D}$ is a negative-definite matrix. Indeed, it is a perpendicular operator, sending $\mathbf{y}$ to a new vector which is perpendicular to $\mathbf{y}$ itself.

Liu (2000) has derived a system of ODEs based on the Jordan algebra:

$$\dot{\mathbf{x}} = [\mathbf{y}, \mathbf{z}, \mathbf{u}] = \mathbf{y} \cdot \mathbf{z}\mathbf{u} - \mathbf{u} \cdot \mathbf{z}\mathbf{y}. \tag{23}$$

The triplet $\mathbf{y}$, $\mathbf{z}$ and $\mathbf{u}$ are functions of $\mathbf{x}$ and t. If $\mathbf{y}$, $\mathbf{z}$ and $\mathbf{u}$ do not depend on t the system is autonomous; otherwise, it is non-autonomous.

From Eq. (19) we can define a new time scale to absorb the time function $q(t)$, such that we have

$$\dot{\mathbf{y}} = \left[\mathbf{I}_n - \frac{\|\mathbf{y}\|^2}{\mathbf{y} \cdot \mathbf{A}\mathbf{y}}\mathbf{A}\right]\mathbf{y}, \tag{24}$$

where for saving notation we also use t to denote the new time and now the superimposed dot denotes the differential with respect to the new time t.

In terms of the Jordan dynamics in Eq. (23) we can write Eq. (24) as

$$\dot{\mathbf{y}} = \left[\frac{\mathbf{A}\mathbf{y}}{\mathbf{y} \cdot \mathbf{A}\mathbf{y}}, \mathbf{y}, \mathbf{y}\right]. \tag{25}$$

3.2 The rotation group $SO(n)$

Obviously, Eq. (25) can be written as

$$\dot{\mathbf{y}} = \left[\mathbf{y} \otimes \frac{\mathbf{A}\mathbf{y}}{\mathbf{y} \cdot \mathbf{A}\mathbf{y}} - \frac{\mathbf{A}\mathbf{y}}{\mathbf{y} \cdot \mathbf{A}\mathbf{y}} \otimes \mathbf{y}\right]\mathbf{y}, \tag{26}$$

where $\mathbf{u} \otimes \mathbf{y}$ denotes the dyadic operation of $\mathbf{u}$ and $\mathbf{y}$, i.e., $(\mathbf{u} \otimes \mathbf{y})\mathbf{z} = \mathbf{y} \cdot \mathbf{z}\mathbf{u}$.

Furthermore, we have

$$\dot{\mathbf{y}} = \frac{1}{\mathbf{y}\cdot\mathbf{A}\mathbf{y}}\left[\mathbf{y}\mathbf{y}^{\mathrm{T}}\mathbf{A} - \mathbf{A}\mathbf{y}\mathbf{y}^{\mathrm{T}}\right]\mathbf{y}. \tag{27}$$

Because the coefficient matrix is skew-symmetric, the Lie-group for the above dynamical system is a rotation group $SO(n)$.

3.3 Generalized Hamiltonian formulation

Let us define

$$\mathbf{J} = \left[\mathbf{y}\otimes\frac{\mathbf{A}\mathbf{y}}{\mathbf{y}\cdot\mathbf{A}\mathbf{y}} - \frac{\mathbf{A}\mathbf{y}}{\mathbf{y}\cdot\mathbf{A}\mathbf{y}}\otimes\mathbf{y}\right], \tag{28}$$

and thus a bracket follows:

$$[f,g] := \boldsymbol{\nabla} f\cdot\mathbf{J}\boldsymbol{\nabla} g \tag{29}$$

for arbitrary functions $f(\mathbf{y})$ and $g(\mathbf{y})$. As being a Poisson bracket, the non-canonical metric $\mathbf{J}$ must be skew-symmetric and satisfies the Jacobi identity, that is,

$$J_{ij} = -J_{ji},\ \ i,j = 1,2,\cdots,n \tag{30}$$

$$J_{i\ell}J_{jk,\ell} + J_{j\ell}J_{ki,\ell} + J_{k\ell}J_{ij,\ell} = 0,\ \ i,j,k = 1,2,\cdots,n, \tag{31}$$

where J_{ij} is the ij-component of $\mathbf{J}$, $J_{jk,\ell}$ denotes $\partial J_{jk}/\partial y_\ell$, and so on. In this formulation $\mathbf{J}$ is allowed to depend on $\mathbf{y}$, and the dimension n is not necessarily restricted to be an even number. The first condition is obvious via Eq. (28); however, the second condition is more complex, which can be proved through a lengthy symbolic operation. Furthermore, if we let $H = \|\mathbf{y}\|^2/2$ be a Hamiltonian function, then Eq. (26) becomes a generalized Hamiltonian system:

$$\dot{\mathbf{y}} = \mathbf{J}\boldsymbol{\nabla} H. \tag{32}$$

3.4 Metric bracket system

Eq. (24) can be written as

$$\dot{\mathbf{y}} = \boldsymbol{\eta}\mathbf{y}, \tag{33}$$

where

$$\boldsymbol{\eta} := \mathbf{I}_n - \frac{\mathbf{A}\mathbf{y}\mathbf{y}^{\mathrm{T}}}{\mathbf{y}\cdot\mathbf{A}\mathbf{y}} \tag{34}$$

is a projection operator because of $\boldsymbol{\eta}^2 = \boldsymbol{\eta}$.

$\boldsymbol{\eta}$ is a singular metric for the following reasons:

$$\det\boldsymbol{\eta} = 0, \tag{35}$$

$$\boldsymbol{\eta}\frac{\mathbf{Ay}}{\mathbf{y}\cdot\mathbf{Ay}} = \mathbf{0}, \tag{36}$$

$$\boldsymbol{\eta} \geq \mathbf{0}. \tag{37}$$

The first indicates that there is at least one zero eigenvalue of $\boldsymbol{\eta}$. In fact, the metric $\boldsymbol{\eta}$ defined by Eq. (34) is a degenerate Riemannian metric. Simultaneously, Eq. (33) becomes

$$\dot{\mathbf{y}} = \boldsymbol{\eta}\boldsymbol{\nabla}H. \tag{38}$$

In terms of the metric bracket,

$$(f,g) := \boldsymbol{\nabla}f\cdot\boldsymbol{\eta}\boldsymbol{\nabla}g \tag{39}$$

defined for arbitrary functions $f(\mathbf{y})$ and $g(\mathbf{y})$, system (38) can be recast to

$$\dot{y}^i = (y^i, H), \quad i = 1,2,\cdots,n. \tag{40}$$

Two functions $f(\mathbf{y})$ and $g(\mathbf{y})$ are said to be involutive, if

$$(f,g) = \boldsymbol{\nabla}f\cdot\boldsymbol{\eta}\boldsymbol{\nabla}g = 0. \tag{41}$$

Let

$$F = \frac{1}{2}\ln\mathbf{y}\cdot\mathbf{Ay}, \tag{42}$$

and by using Eq. (36) it follows that

$$\boldsymbol{\eta}\boldsymbol{\nabla}F = \mathbf{0}; \tag{43}$$

hence, one has

$$(g,F) = \boldsymbol{\nabla}g\cdot\boldsymbol{\eta}\boldsymbol{\nabla}F = 0 \tag{44}$$

for every functions $g(\mathbf{y})$. It means that F is involutive with every functions. We may call such $F(\mathbf{y})$ a Casimir function of the metric bracket system. It is apparent that the existence of the Casimir function confines the trajectory of $\mathbf{y}$ on a hypersurface as defined by $\|\mathbf{y}\| = \|\mathbf{r}_0\|$.

4 Structure preserving algorithms

4.1 The first structure preserving algorithm

Based on the above results we can develop the first structure preserving algorithm (SPA1) to solve Eq. (2):
(i) Select a suitable value of $0 \leq \gamma < 1$ and give an initial $\mathbf{x}_0$.
(ii) Calculate $\mathbf{r}_0 = \mathbf{B}\mathbf{x}_0 - \mathbf{b}$ and $\mathbf{y}_0 = \mathbf{r}_0$.
(iii) For $k = 1, 2, \ldots$, we repeat the following computations:

$$\begin{aligned}
&\beta_{k-1} = (1-\gamma)\frac{(\mathbf{y}_{k-1}^{\mathrm{T}}\mathbf{A}\mathbf{y}_{k-1})^2}{\|\mathbf{y}_{k-1}\|^2\|\mathbf{A}\mathbf{y}_{k-1}\|^2},\\
&\mathbf{x}_k = \mathbf{x}_{k-1} - \beta_{k-1}\frac{\|\mathbf{y}_{k-1}\|^2}{\mathbf{y}_{k-1}^{\mathrm{T}}\mathbf{A}\mathbf{y}_{k-1}}\mathbf{B}^{\mathrm{T}}\mathbf{r}_{k-1},\\
&\mathbf{y}_k = \mathbf{y}_{k-1} + \beta_{k-1}\left[\mathbf{I}_n - \frac{\|\mathbf{y}_{k-1}\|^2}{\mathbf{y}_{k-1}^{\mathrm{T}}\mathbf{A}\mathbf{y}_{k-1}}\mathbf{A}\right]\mathbf{y}_{k-1},\\
&\mathbf{y}_k = \frac{\|\mathbf{y}_{k-1}\|}{\|\mathbf{y}_k\|}\mathbf{y}_k, \quad (\textbf{preserving the length of } \mathbf{y}),\\
&\mathbf{r}_k = \mathbf{B}\mathbf{x}_k - \mathbf{b},\\
&\mathbf{R}_k = \mathbf{B}^{\mathrm{T}}\mathbf{r}_k.
\end{aligned} \tag{45}$$

If $\mathbf{x}_k$ converges according to a given stopping criterion $\|\mathbf{R}_k\| < \varepsilon$ then stop; otherwise, go to step (iii). In the above we have inserted $\beta_k = q\Delta t$ by

$$\beta_k = (1-\gamma)\frac{(\mathbf{y}_k^{\mathrm{T}}\mathbf{A}\mathbf{y}_k)^2}{\|\mathbf{y}_k\|^2\|\mathbf{A}\mathbf{y}_k\|^2}, \tag{46}$$

according to Liu (2011a) with $\mathbf{r}_k$ being replaced by $\mathbf{y}_k$, where $0 \leq \gamma < 1$ is a relaxation parameter.

4.2 The second structure preserving algorithm

Suppose that

$$\mathbf{y}_k = \alpha_{k-1}\mathbf{y}_{k-1} + \beta_{k-1}\left[\mathbf{I}_n - \frac{\|\mathbf{y}_{k-1}\|^2}{\mathbf{y}_{k-1}^{\mathrm{T}}\mathbf{A}\mathbf{y}_{k-1}}\mathbf{A}\right]\mathbf{y}_{k-1}, \tag{47}$$

where α_{k-1} is a factor to be determined, such that the length of $\mathbf{y}_k$ is preserved:

$$\|\mathbf{y}_k\|^2 = \|\mathbf{y}_{k-1}\|^2. \tag{48}$$

Inserting Eq. (47) into Eq. (48) we can derive

$$\alpha_{k-1}=\sqrt{1+\beta_{k-1}^2\left[1-\frac{\|\mathbf{y}_{k-1}\|^2\|\mathbf{A}\mathbf{y}_{k-1}\|^2}{(\mathbf{y}_{k-1}^{\mathrm{T}}\mathbf{A}\mathbf{y}_{k-1})^2}\right]}. \tag{49}$$

Based on the above results we can derive the second structure preserving algorithm (SPA2) to solve Eq. (2):
(i) Select a suitable value of $0\leq\gamma<1$ and give an initial $\mathbf{x}_0$.
(ii) Calculate $\mathbf{r}_0=\mathbf{B}\mathbf{x}_0-\mathbf{b}$ and $\mathbf{y}_0=\mathbf{r}_0$.
(iii) For $k=1,2,\ldots$, we repeat the following computations:

$$\begin{aligned}
&\beta_{k-1}=(1-\gamma)\frac{(\mathbf{y}_{k-1}^{\mathrm{T}}\mathbf{A}\mathbf{y}_{k-1})^2}{\|\mathbf{y}_{k-1}\|^2\|\mathbf{A}\mathbf{y}_{k-1}\|^2},\\
&\alpha_{k-1}=\sqrt{1+\beta_{k-1}^2\left[1-\frac{\|\mathbf{y}_{k-1}\|^2\|\mathbf{A}\mathbf{y}_{k-1}\|^2}{(\mathbf{y}_{k-1}^{\mathrm{T}}\mathbf{A}\mathbf{y}_{k-1})^2}\right]},\\
&\mathbf{x}_k=\mathbf{x}_{k-1}-\beta_{k-1}\frac{\|\mathbf{y}_{k-1}\|^2}{\mathbf{y}_{k-1}^{\mathrm{T}}\mathbf{A}\mathbf{y}_{k-1}}\mathbf{B}^{\mathrm{T}}\mathbf{r}_{k-1},\\
&\mathbf{y}_k=\alpha_{k-1}\mathbf{y}_{k-1}+\beta_{k-1}\left[\mathbf{I}_n-\frac{\|\mathbf{y}_{k-1}\|^2}{\mathbf{y}_{k-1}^{\mathrm{T}}\mathbf{A}\mathbf{y}_{k-1}}\mathbf{A}\right]\mathbf{y}_{k-1},\\
&\mathbf{r}_k=\mathbf{B}\mathbf{x}_k-\mathbf{b},\\
&\mathbf{R}_k=\mathbf{B}^{\mathrm{T}}\mathbf{r}_k.
\end{aligned} \tag{50}$$

If $\mathbf{x}_k$ converges to satisfy a given stopping criterion $\|\mathbf{R}_k\|<\varepsilon$ then stop; otherwise, go to step (iii).

5 Numerical examples

In order to investigate the influence from noise to the novel algorithms, we subject the right-hand side data $\mathbf{b}$ of Eq. (2) by random noise:

$$\tilde{b}_i=b_i+\sigma R(i),\quad i=1,\ldots,n, \tag{51}$$

where $R(i)$ are Gaussian random numbers in $[-1,1]$, and σ is the intensity of noise.

5.1 Example 1

In this example we consider a two-dimensional but highly ill-conditioned linear system:

$$\begin{bmatrix} 2 & 6 \\ 2 & 6.00001 \end{bmatrix} \begin{bmatrix} x \\ y \end{bmatrix} = \begin{bmatrix} 8 \\ 8.00001 \end{bmatrix}. \tag{52}$$

The condition number of this system is $\mathrm{Cond}(\mathbf{C}) = 1.59 \times 10^{13}$, where $\mathbf{C} = \mathbf{B}^{\mathrm{T}}\mathbf{B}$ and $\mathbf{B}$ denotes the coefficient matrix . The exact solution is $(x,y) = (1,1)$.

No matter what regularization parameter is used in the Tikhonov regularization method for the above equation, an incorrect solution of $(x,y) = (1356.4, -450.8)$ is obtained by the Tikhonov regularization method.

Now we fix the noise to be $\sigma = 0.01$, $\varepsilon = 10^{-9}$ and starting from an initial condition $(x_0, y_0) = (0.8, 0.5)$. The SDM led to an incorrect result $(x,y) = (415.8, -137.3)$. Then we apply the present SPA1 with $\gamma = 0.05$ to this problem under $\varepsilon = 10^{-8}$, which led to an approximate solution of $(x,y) = (0.97, 1.01)$ through 9 iterations. The residual error of SPA1 is shown in Fig. 2. We also apply the SPA2 with $\gamma = 0.04$ to this problem, which led to an approximate solution of $(x,y) = (0.97, 1.01)$ through 8 iterations. The residual error of SPA2 is shown in Fig. 2. When the SDM is vulnerable to the disturbance of noise for the above ill-posed linear system, the SPAs can work very well against the disturbance of noise.

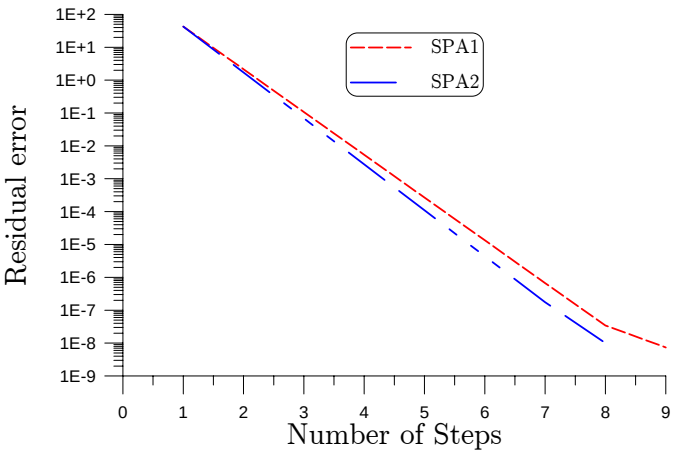

Figure 2: For example 1 comparing the residual errors obtained by the SPA1 and SPA2.

5.2 Example 2

The Hilbert matrix

$$B_{ij} = \frac{1}{i+j-1} \tag{53}$$

is notoriously ill-conditioned. It is known that the condition number of Hilbert matrix grows as $e^{3.5n}$ when n is very large. For the case with $n = 200$ the condition number is extremely huge to the order 10^{348}.

We take $n = 200$, and suppose that $x_i = 1,\ i = 1\ldots,200$ is the exact solution. The noise is $\sigma = 0.01$, $\varepsilon = 10^{-4}$ and we start from an initial condition $x_i = 0.5,\ i = 1\ldots,200$. The RSDM with $\gamma = 0.25$ led to a less accurate result, whose residual error is shown in Fig. 3(a), and the numerical error is shown in Fig. 3(b). The maximum error is 0.1745. Then we apply the SPA1 and SPA2 with the same $\gamma = 0.25$ to this problem, which led to good approximate solutions as shown in Fig. 3(b). The maximum error of SPA1 is 0.071, while the maximum error of SPA2 is 0.068. The residual errors of SPA1 and SPA2 are shown in Fig. 3(a), of which the SPA2 converges faster than the other two algorithms.

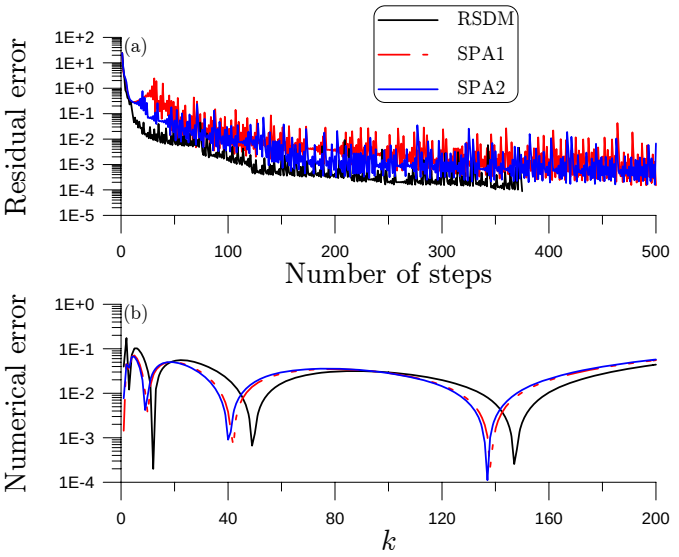

Figure 3: For example 2: (a) comparing the residual errors obtained by the RSDM and the present methods SPA1 and SPA2, and (b) comparing the numerical errors.

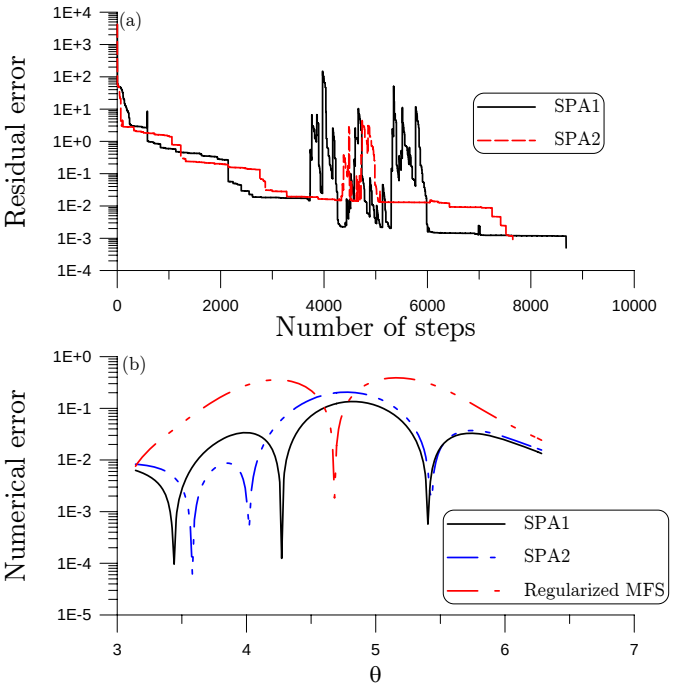

Figure 4: For example 3: (a) comparing the residual errors obtained by SPA1 and SPA2, and (b) comparing the numerical errors obtained by SPA1, SPA2, and the regularized MFS of Wei, Hon and Ling (2007).

5.3 Example 3

We solve the Cauchy problem of the Laplace equation under overspecified boundary conditions on the upper contour:

$$\Delta u = u_{rr} + \frac{1}{r}u_r + \frac{1}{r^2}u_{\theta\theta} = 0, \quad r < \rho, \quad 0 \le \theta \le 2\pi, \tag{54}$$

$$u(\rho,\theta) = h(\theta), \quad 0 \le \theta \le \pi, \tag{55}$$

$$u_n(\rho,\theta) = g(\theta), \quad 0 \le \theta \le \pi, \tag{56}$$

where $h(\theta)$ and $g(\theta)$ are given functions, and $\rho = \rho(\theta)$ is a given contour to describe the boundary shape. The contour in the polar coordinates is specified by $\Gamma = \{(r,\theta) | r = \rho(\theta),\ 0 \le \theta \le 2\pi\}$, which is the boundary of the problem domain Ω, and n denotes the normal direction.

In the potential theory, it is well known that the method of fundamental solutions (MFS) can be used to solve the Laplacian problems when a fundamental solution

is known [Kupradze and Aleksidze (1964)]. In the MFS the trial solution of u at the field point $\mathbf{z} = (r\cos\theta, r\sin\theta)$ can be expressed as a linear combination of the fundamental solutions $U(\mathbf{z},\mathbf{s}_j)$:

$$u(\mathbf{z}) = \sum_{j=1}^{n} c_j U(\mathbf{z},\mathbf{s}_j), \quad \mathbf{s}_j \in \Omega^c, \tag{57}$$

where n is the number of source points, c_j are the unknown coefficients, $\mathbf{s}_j$ are the source points, and Ω^c is the complementary set of Ω. For the Laplace equation (54) we have the fundamental solutions:

$$U(\mathbf{z},\mathbf{s}_j) = \ln r_j, \quad r_j = \|\mathbf{z}-\mathbf{s}_j\|. \tag{58}$$

In a practical application of MFS, frequently the source points are uniformly located on a circle with a radius R, such that after imposing the boundary conditions (55) and (56) on Eq. (57) we can obtain a linear equations system:

$$\mathbf{B}\mathbf{x} = \mathbf{b}, \tag{59}$$

where

$$\begin{aligned}
&\mathbf{z}_i = (z_i^1, z_i^2) = (\rho(\theta_i)\cos\theta_i, \rho(\theta_i)\sin\theta_i),\\
&\mathbf{s}_j = (s_j^1, s_j^2) = (R\cos\theta_j, R\sin\theta_j),\\
&B_{ij} = \ln\|\mathbf{z}_i-\mathbf{s}_j\|, \quad \text{if } i \text{ is odd},\\
&B_{ij} = \frac{\eta(\theta_i)}{\|\mathbf{z}_i-\mathbf{s}_j\|^2}\Big(\rho(\theta_i) - s_j^1\cos\theta_i - s_j^2\sin\theta_i\\
&\qquad -\frac{\rho'(\theta_i)}{\rho(\theta_i)}[s_j^1\sin\theta_i - s_j^2\cos\theta_i]\Big), \text{if } i \text{ is even},\\
&\mathbf{x} = (c_1,\ldots,c_n)^{\mathrm{T}}, \quad \mathbf{b} = (h(\theta_1), g(\theta_1), \ldots, h(\theta_m), g(\theta_m))^{\mathrm{T}},
\end{aligned} \tag{60}$$

in which $n = 2m$, and

$$\eta(\theta) = \frac{\rho(\theta)}{\sqrt{\rho^2(\theta) + [\rho'(\theta)]^2}}. \tag{61}$$

This example imposes a great challenge to test the efficiency of linear equations solver, because the Cauchy problem is highly ill-posed. We fix $n = 38$ and employ a circle with a constant radius $R = 15$ to distribute the source points. We apply both the SPA1 and the SPA2 with $\gamma = 0.05$ to solve the linear system (59) under a convergence criterion $\varepsilon = 10^{-3}$, where a noise with an intensity $\sigma = 10\%$ is imposed on the given data. Under the initial guess with $x_i = 0.1$, the residual errors

are plotted in Fig. 4(a), where the SPA1 is convergent with 8682 iterations and the SPA2 is convergent with 7650 iterations. Along the lower half contour $\rho(\theta) = \sqrt{10-6\cos(2\theta)},\ \pi \le \theta < 2\pi$, in Fig. 4(b) we compare the numerical solutions obtained by SPA1 and SPA2 with the data given by $u = \rho^2\cos(2\theta),\ \pi \le \theta < 2\pi$. For the purpose of comparison with the regularized MFS proposed by Wei, Hon and Ling (2007), we first plot the L-curve and thus take the optimal value of α to be $\alpha = 8.7437 \times 10^{-6}$. Through the regularized MFS, the maximum error is found to be 0.39 as shown in Fig. 4(b). We can observe that the results obtained by the SPA1 and SPA2 are very close to the exact one, where the maximum error for the SPA1 is 0.14, while that for the SPA2 is 0.21. Obviously, as shown in Fig. 4(b) the SPA2 is more accurate than the SPA1, and the regularized MFS.

5.4 Example 4

When the backward heat conduction problem (BHCP) is considered in a spatial interval of $0 < x < \ell$ by subjecting to the boundary conditions at two ends of a slab:

$$u_t(x,t) = \alpha u_{xx}(x,t),\ \ 0 < t < T,\ \ 0 < x < \ell, \tag{62}$$

$$u(0,t) = u_0(t),\ \ u(\ell,t) = u_\ell(t), \tag{63}$$

we solve u under a final time condition:

$$u(x,T) = u^T(x). \tag{64}$$

The fundamental solution of Eq. (62) is given as follows:

$$K(x,t) = \frac{H(t)}{2\sqrt{\alpha\pi t}} \exp\left(\frac{-x^2}{4\alpha t}\right), \tag{65}$$

where $H(t)$ is the Heaviside function.

The method of fundamental solutions (MFS) has a broad application in engineering computations. In the MFS the solution of u at the field point $\mathbf{z} = (x,t)$ can be expressed as a linear combination of the fundamental solutions $U(\mathbf{z},\mathbf{s}_j)$:

$$u(\mathbf{z}) = \sum_{j=1}^{n} c_j U(\mathbf{z},\mathbf{s}_j),\ \ \mathbf{s}_j = (\eta_j,\tau_j) \in \Omega^c, \tag{66}$$

where n is the number of source points, c_j are unknown coefficients, and $\mathbf{s}_j$ are source points being located in the complement Ω^c of $\Omega = [0,\ell] \times [0,T]$. For the heat conduction equation we have

$$U(\mathbf{z},\mathbf{s}_j) = K(x-\eta_j, t-\tau_j). \tag{67}$$

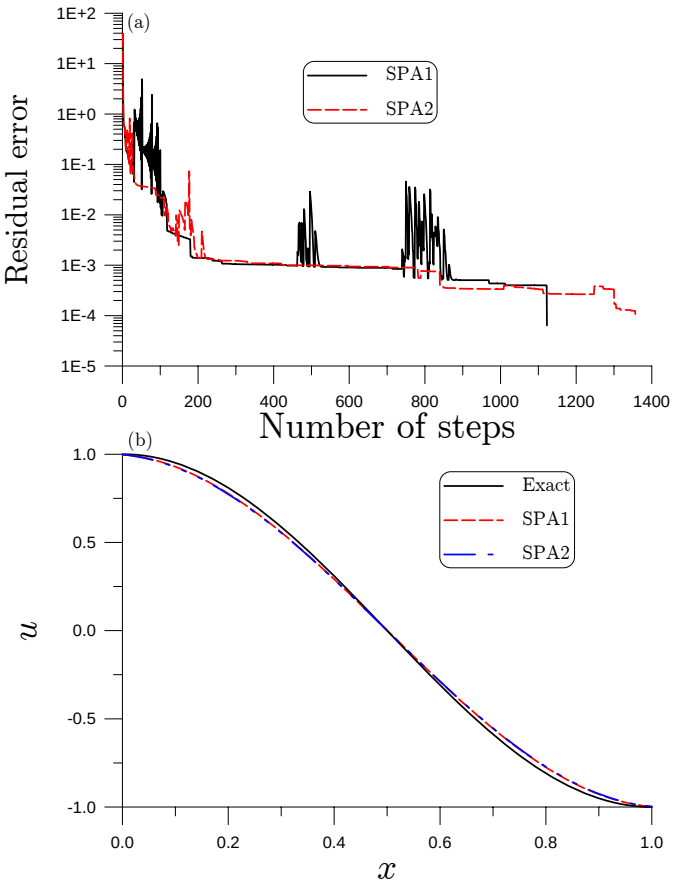

Figure 5: For example 4: (a) comparing the residual errors obtained by SPA1 and SPA2, and (b) comparing the numerical solutions with the exact one.

It is known that the distribution of source points in the MFS has a great influence on the accuracy and stability. In a practical application of MFS to solve the BHCP, the source points are uniformly located on two vertical straight lines parallel to the t-axis and one horizontal line over the final time, which was adopted by Hon and Li (2009) and Liu (2011b), showing a large improvement than the line location of source points below the initial time. After imposing the boundary conditions and the final time condition on Eq. (66) we can obtain a linear equations system:

$$\mathbf{Bx} = \mathbf{b}, \tag{68}$$

where

$$B_{ij} = U(\mathbf{z}_i, \mathbf{s}_j), \quad \mathbf{x} = (c_1, \cdots, c_n)^{\mathrm{T}},$$
$$\mathbf{b} = (u_\ell(t_i),\ i = 1, \ldots, m_1; u^T(x_j),\ j = 1, \ldots, m_2; u_0(t_k),\ k = m_1, \ldots, 1)^{\mathrm{T}}, \tag{69}$$

and $n = 2m_1 + m_2$.

Since the BHCP is highly ill-posed, the ill-condition of the coefficient matrix $\mathbf{B}$ in Eq. (68) is serious. To overcome the ill-posedness of Eq. (68) we can use the new method to solve this problem. Here we compare the numerical solution with an exact solution:

$$u(x,t) = \cos(\pi x)\exp(-\pi^2 t).$$

For the case with $T = 1$ the value of final time data is in the order of 10^{-4}, which is much small in a comparison with the value of the initial temperature $u_0(x) = \cos(\pi x)$ to be retrieved, which is $O(1)$. We solve this problem by the SPA1 and SPA2 with $\gamma = 0.05$. The initial guess is $x_i = 1$. As shown in Fig. 5(a), both the SPA1 and the SPA2 converge very fast with respectively 1123 and 1364 iterations under the convergence criterion $\varepsilon = 10^{-4}$. We have added a relative random noise with an intensity $\sigma = 10\%$ on the final time data, of which we compare the numerical solutions with the exact initial data in Fig. 5(b), of which the maximum error is smaller than 0.035 for the SPA1, and 0.038 for the SPA2. It indicates that the present iterative algorithms are rather robust against noise, and which can provide rather accurate numerical results.

6 Conclusions

In the present paper we have extended the classical steepest descent method and developed two structure preserving algorithms, SPA1 and SPA2, which can largely accelerate the convergence speed in the numerical solution of an ill-posed linear system $\mathbf{Bx} = \mathbf{b}$. In the framework of the future cone we have found four structures in the scaled residual dynamics, namely the Jordan dynamics, the Lie-group $SO(n)$, the generalized Hamiltonian formulation, as well as a metric bracket system. An extra variable $\mathbf{y}$ on $\mathbb{S}^{n-1}$ was introduced, of which the two simple algorithms SPA1 and SPA2 can preserve the length of $\mathbf{y}$. Obviously, the present SPA1 and SPA2 can be implemented easily and effectively used to solve the linear inverse problems.

Acknowledgement: Taiwan's National Science Council project NSC-100-2221-E-002-165-MY3 and the 2011 Outstanding Research Award, as well as the 2011

Taiwan Research Front Award from Thomson Reuters granted to the first author are highly appreciated. The work at UCI was supported by the Vehicle Technology Division of ARL, under a cooperative agreement with UCI.

References

Barzilai, J.; Borwein, J. M. (1988): Two point step size gradient methods. *IMA J. Numer. Anal.*, vol. 8, pp. 141-148.

Hon, Y. C.; Li, M. (2009): A discrepancy principle for the source points location in using the MFS for solving the BHCP. *Int. J. Comput. Meth.*, vol. 6, pp. 181-197.

Kunisch, K.; Zou, J. (1998): Iterative choices of regularization parameters in linear inverse problems. *Inverse Problems*, vol. 14, pp. 1247-1264.

Kupradze, V. D.; Aleksidze, M. A. (1964): The method of functional equations for the approximate solution of certain boundary value problems. *USSR Comput. Math. Math. Phy.*, vol. 4, pp. 82-126.

Liu, C.-S. (2000): A Jordan algebra and dynamic system with associator as vector field. *Int. J. Non-Linear Mech.*, vol. 35, pp. 421-429.

Liu, C.-S. (2001): Cone of non-linear dynamical system and group preserving schemes. *Int. J. Non-Linear Mech.*, vol. 36, pp. 1047-1068.

Liu, C.-S. (2011a): A revision of relaxed steepest descent method from the dynamics on an invariant manifold. *CMES: Computer Modeling in Engineering & Sciences*, vol. 80, pp. 57-86.

Liu, C.-S. (2011b): The method of fundamental solutions for solving the backward heat conduction problem with conditioning by a new post-conditioner. *Num. Heat Transfer, B: Fundamentals*, vol. 60, pp. 57-72.

Liu, C.-S. (2012a): Modifications of steepest descent method and conjugate gradient method against noise for ill-posed linear system. *Commun. Numer. Anal.*, vol. 2012, Article ID cna-00115, 24 pages.

Liu, C.-S. (2012b): Optimally scaled vector regularization method to solve ill-posed linear problems. *Appl. Math. Comp.*, vol. 218, pp. 10602-10616.

Liu, C.-S. (2012c): A globally optimal iterative algorithm to solve an ill-posed linear system. *CMES: Computer Modeling in Engineering & Sciences*, vol. 84, pp. 383-403.

Liu, C.-S. (2012d): A dynamical Tikhonov regularization for solving ill-posed linear algebraic systems. *Acta Appl. Math.*, 10.1007/s10440-012-9766-3.

Liu, C.-S. (2012e): Optimally generalized regularization methods for solving linear inverse problems. *CMC: Computers, Materials & Continua*, vol. 29, pp. 103-

127.

Liu, C.-S. (2012f): An optimal tri-vector iterative algorithm for solving ill-posed linear inverse problems. *Inv. Prob. Sci. Eng.*, DOI:10.1080/17415977.2012.717077.

Liu, C.-S.; Atluri, S. N. (2009a): A Fictitious time integration method for the numerical solution of the Fredholm integral equation and for numerical differentiation of noisy data, and its relation to the filter theory. *CMES: Computer Modeling in Engineering & Sciences*, vol. 41, pp. 243-261.

Liu, C.-S.; Atluri, S. N. (2009b): A highly accurate technique for interpolations using very high-order polynomials, and its applications to some ill-posed linear problems. *CMES: Computer Modeling in Engineering & Sciences*, vol. 43, pp. 253-276.

Liu, C.-S.; Atluri, S. N. (2011): An iterative method using an optimal descent vector, for solving an ill-conditioned system $\mathbf{Bx} = \mathbf{b}$, better and faster than the conjugate gradient method. *CMES: Computer Modeling in Engineering & Sciences*, vol. 80, pp. 275-298.

Liu, C.-S.; Chang, C. W. (2009): Novel methods for solving severely ill-posed linear equations system. *J. Marine Sci. Tech.*, vol. 17, pp. 216-227.

Liu, C.-S.; Hong, H. K.; Atluri, S. N. (2010): Novel algorithms based on the conjugate gradient method for inverting ill-conditioned matrices, and a new regularization method to solve ill-posed linear systems. *CMES: Computer Modeling in Engineering & Sciences*, vol. 60, pp. 279-308.

Resmerita, E. (2005): Regularization of ill-posed problems in Banach spaces: convergence rates. *Inverse Problems*, vol. 21, pp. 1303-1314.

Tikhonov, A. N.; Arsenin, V. Y. (1997): Solutions of Ill-Posed Problems. John-Wiley & Sons, New York.

Wang, Y.; Xiao, T. (2001): Fast realization algorithms for determining regularization parameters in linear inverse problems. *Inverse Problems*, vol. 17, pp. 281-291.

Wei, T.; Hon, Y. C.; Ling, L. (2007): Method of fundamental solutions with regularization techniques for Cauchy problems of elliptic operators. *Eng. Anal. Bound. Elem.*, vol. 31, pp. 373-385.

Xie, J.; Zou, J. (2002): An improved model function method for choosing regularization parameters in linear inverse problems. *Inverse Problems*, vol. 18, pp. 631-643.